J Porous Mater (2017) 24:1237–1246
DOI 10.1007/s10934-017-0364-7

B–SBA-15–SO_3H: a versatile mesoporous catalyst

Beyhan Erdem[1] · **Çağla Azko**[1]

Published online: 28 January 2017

Abstract Novel approach was developed towards the synthesis of heterogeneous mesoporous B–SBA-15–SO_3H acid catalysts. That is: B–SBA-15 materials were hydrothermally synthesized by using three different boron sources (boric acid, trisiopropylborate and potassium borohydride) and then post-synthetically functionalized with sulfonic acid to test their catalytic activity for the esterification of propionic acid with methanol. Mesoporous and amorphous character of the materials as well as the incorporation of the boron into the framework were verified by XRD, N_2-adsorption/desorption, ICP–OES, SEM and FT-IR techniques. All of the boron incorporated acid catalysts showed better activity than pure SBA-15–SO_3H for methyl propionate synthesis. Combining the advantageous of hydrothermal synthesis and post functionalization, the obtained B–SBA-15–SO_3H catalysts should present versatile catalytic properties in terms of both catalytic activity and reusability. Boron incorporation and post functionalization encourage the structural configuration, since the grafted catalytically active groups may experience similar environments and be isolated from each other.

Keywords Boron · SBA-15 · Hydrothermal synthesis · Post functionalization · Mesoporous acid catalyst

✉ Beyhan Erdem
gbeyhan@uludag.edu.tr

[1] Department of Chemistry, Faculty of Science and Arts, Uludag University, 16059 Bursa, Turkey

1 Introduction

The mesoporosity of silica-based materials has come to the forefront as a new and exciting research field of great scientific and technological importance in heterogeneous catalysis. The ability to design both the size and wall surface characters of the pores is important towards imposing a framework for tailoring and fine-tuning catalytic activities [1]. There is no doubt that the presence of these mesopores combined with acidic properties opens up new possibilities for processing and/or producing large molecules [2]. Generally, incorporation of heteroatom such as Al, Ti, Cu and V within the silica framework of mesoporous materials such as MCM-41 and MCM-48 has been implemented in order to create catalytically active sites, ion-exchange capacity and hence their catalytic activity. However, it is very difficult to introduce the metal ions in the silica framework of SBA-15 directly due to the facile dissociation of metal–O–Si bonds under strong acidic hydrothermal conditions. For example, the ion-exchange, catalytic and adsorptive properties of alumino-silicate molecular sieves originate from acidic sites which arise from the presence of accessible hydroxyl groups associated with tetrahedral aluminum in the silica matrix [3].

Oberhagemann et al. [4], first synthesized highly ordered B–MCM-41 and found that B–MCM-41 is a boron containing analog to aluminosilicate MCM-41 with [BO_4] tetrahedral units as parts of the silicate framework and boron changes its coordination to trigonal planar upon calcination. In the course of calcination most of the boron is removed from the framework and resides within the channel-like pores where it becomes hydrated after exposure to atmospheric humidity. Trong On et al. [2] synthesized B–MCM-41 hydrothermally and found that adding boron to the synthesis gel increases the long-range ordering of the

materials compared to that of the pure silica analogue. A problem of this type of catalyst is the hybrid acid sites and deconcentrated acidity, leading to low selectivity toward the targeted product. Thus, mesoporous materials functionalized by propyl-sulfonic groups, arenesulfonic groups, carboxylate groups and peroxycarboxylic acid groups were developed for a high accessibility of the active site and concentrated acid strength, which were promising catalysts for a variety of reaction such as the esterification, etherification and condensation reactions [5].

The inorganic part (polymeric silicate framework) of the surface modified hybrid mesoporous materials provides structural, thermal and mechanical stability whereas the pendent organic species permit flexible control of interfacial and bulk properties. Mesoporous materials are, in general, hydrophilic because of the surface hydroxyl (Si–OH) groups. Organo-functionalization modifies the surface properties making them relatively more hydrophobic. The hydrophobic nature of the active sites' environment can be exploited to perform reactions, which are outside the reach of the other inorganic solid acid catalysts.

Organo-functionalization of the internal surfaces of mesoporous silicates can be achieved either by covalent grafting of various organic moieties onto the channel walls or by incorporating functionalities directly during the synthesis. The grafting process has been widely applied to anchor desired organic functional groups via condensation with surface silanol groups of the mesoporous silicate. However, it is somewhat difficult to control the concentration and distribution of organic moieties on the silicate surface mainly due to non-uniform presence of silanol groups in different mesoporous samples.

The direct synthesis approach is based on the co-condensation of one tetraalkoxysilane with trialkoxyorganosilane precursors in a templating environment. The tetraalkoxysilane precursor acts as a building block to create the mesoporous silicate framework, whereas the trialkoxyorganosilanes function as both framework silicate units and pendent organic functional groups. This one-step synthesis procedure can produce mesoporous silicates with high loading and homogeneous surface coverage of organic functional groups. However, in the direct synthesis approach, organic functional groups may be damaged or destroyed during the template removal process; the secondary silylation technique (grafting technique) seems to offer a better alternative for preparing mesoporous acid catalysts [6].

In this paper, we report an effective and convenient method which combines the direct and the post synthesis. In this method, to prepare sulfonic acid functionalized mesoporous boron silicate, B–SBA-15–SO_3H, three different boron sources (boric acid, trisiopropylborate and potassium borohydride) were added into the initial reaction mixture in strongly acidic media just as in the case of direct synthesis; when the B–SBA-15 mesostructure was formed after hydrothermal treatment and calcination, 3-mercaptopropyltrimethoxysilane as organoalkoxysilane precursor was grafted to the mesoporous B–SBA-15. While doing this, we were inspired of molecular spacer approach. That is; for catalytic applications of functionalized mesoporous silica, it is important to establish molecular scale structure–property relationships. This process is greatly facilitated if the grafted catalytically active groups experience similar environments and are isolated from each other [7]. The obtained catalysts were tested in the esterification of propionic acid with methanol and the activity of these new materials was compared to that of SBA-15–SO_3H.

2 Experimental

2.1 Catalyst preparation

Firstly, B–SBA-15 materials were prepared according to hydrothermal procedure described by Grieken et al. [8], by using three different boron sources such as boric acid ($B(OH)_3$, Aldrich), triisopropyl borate ($(((CH_3)_2CHO)_3B$, Aldrich) and potassium borohydride (KBH_4, Aldrich). In a typical synthesis, 4 g of Pluronic P123 was dissolved under stirring in 125 g of 1.9 M HCl. After heating up the solution from room temperature to 40 °C, boron precursors were added separately without adding the boron source to one of the samples. Subsequently, 8.5 g TEOS (Aldrich) was added obtaining a SiO_2/B_2O_3 mole ratio in the synthesis gel equal to 30. The resultant solutions were stirred for 24 h at 40 °C, followed by aging at 90 °C in the Teflon cups for 24 h under static conditions. The solid products were recovered by filtration and dried at 60 °C overnight. Then, the template was removed by calcinations at 500 °C for 6 h.

Secondly, 2 g of all of the samples were kept at 100 °C for an hour in a vacuum and then refluxed with dry toluene and 3-mercaptopropyltrimethoxysilane (Aldrich) for 20 h. After filtrating, the samples were soxhlet extracted with dichloromethane to remove the non-reacting sections of the functional groups. The samples were dried at 40 °C, treated with H_2O_2 to oxidize the –SH groups to –SO_3H groups.

2.2 Characterization

Nitrogen sorption analyses were measured at 77 K with Quantachrome Autosorb 1 C sorption analyzer. Before the measurements, the samples were degassed at 200 °C in vacuum for 5 h. Surface areas were calculated using the Brunauer–Emmet–Teller (BET) method over the range $p/p_o = 0.03–0.2$, where a linear relationship is maintained. Pore size distributions were calculated using the

Barrett–Joyner–Halenda (BJH) method applied to the desorption branch of the isotherm. LA-XRD patterns were collected using a Bruker 4-circle diffractometer equipped with a Cu sealed point source and a Gobel Mirror optic to generate a 2D-collimated parallel beam (divergence ca. 0.03 and a lateral length of 18 mm) and an anti-scatter slit to remove background. Typically, the data were collected from 0.5° to 3° (2θ) and from 10° to 50° (2θ) at 40 kV and 40 mA for low and high angle XRD, respectively. The morphology of the materials was studied using a Zeiss Supra 50VP model SEM. A Thermo Nicolet 6700 series infrared spectrometer was used for FT-IR analysis in normal transmission mode with a KBr detector over the range of 4000–400 cm^{-1} at a resolution of 8 cm^{-1} averaged over 32 scans. The acid exchange capacities of the SBA-15–SO_3H, SBA-15–SO_3H–$B(OH)_3$, SBA-15–SO_3H–TIB, SBA-15–SO_3H–KBH_4 were measured by means of titration, using sodium chloride as exchange agent. In a typical experiment, 0.05 g of solid acid catalyst was added to 10 g of aqueous solution of sodium chloride (2 M). The resulting suspension was allowed to equilibrate and thereafter titrated potentiometrically by dropwise addition of 0.01 N NaOH (aq).

2.3 Catalytic test

The esterification of propionic acid with methanol was carried out in an isothermal glass reactor equipped with a heating jacket the temperature of which was controlled within ±0.1 °C. Stoichiometric ratio of propionic acid to methanol was (1:1) in the experiments performed at 333 K. 1,4-dioxane was used as solvent in all experiments. In a typical run, catalyst (about 0.5 g), methanol and dioxane of known amount were charged into the reactor and preheated to the reaction temperature and the esterification was commenced by adding preheated propionic acid into the mixture. This was considered as the zero time for a run. The total liquid volume was 100 mL. Samples were withdrawn from reactor medium at certain time intervals and then analyzed by titration with 0.1 M sodium hydroxide to determine the amount of unreacted acid. To determine the reusability of the boron incorporated (by $B(OH)_3$ and $((CH_3)_2CHO)_3B$) catalysts, the esterification reactions were repeated three times consecutively with the same catalyst. In these experiments, after the catalyst was recovered from reaction cycle, it was washed extensively with deionized water and dried under vacuum at 333 K before starting the experiment with a new cycle of fresh reactants.

3 Results and discussion

Figure 1 shows the XRD diffraction patterns of the catalyst samples of SBA-15–SO_3H–$B(OH)_3$, SBA-15–SO_3H–TIB, SBA-15–SO_3H–KBH_4 prepared from $B(OH)_3$, $((CH_3)_2CHO)_3B$ and KBH_4, respectively and pure silica catalyst SBA-15–SO_3H. All the catalysts displayed a well-resolved pattern with a sharp peak at 2θ value of 0.9 (Fig. 1) and two small peaks at about 1.6 and 1.8 (the inset of Fig. 1) that matched well with reported patterns for mesoporous materials. The above peaks are indexed to the (100), (110) and (200) reflections of the 2D hexagonal mesostructure with space group p6mm [9]. Presence of all the above peaks for the catalysts confirms that the hexagonal structure is retained after boron incorporation. It is important to mention that the quality of the XRD pattern and the

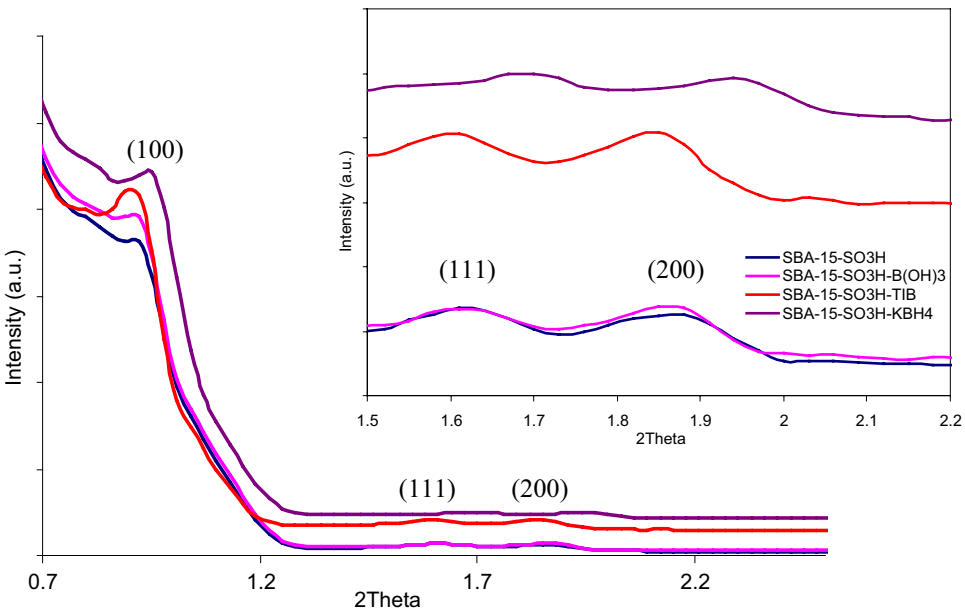

Fig. 1 Low-angle XRD spectra for bare SBA-15–SO_3H and boron incorporated SBA-15–SO_3H samples. The *inset* shows the highlight of 2 theta region between 1.5 and 2.2

position of the main peak may vary significantly, depending on the synthesis conditions, type of silicon and boron sources, and the chain length of the organic template used [2]. The SBA-15–SO_3H–KBH_4 sample yielded a higher quality XRD pattern compared to the other samples. The (100) peak is sharper and more intense. This suggests that using KBH_4 as boron source in the synthesis gel increases the long-range ordering of the material. When the ions having the opposite charge with the colloidal particles are adsorbed on the surface, the charges of the particles and consequently the repulsive force between them are reduced [10]. For this reason, when we use KBH_4 as boron source, long-range ordering can be better because of its charged nature. The stability of the Si–O–B increases with the electrostatic character of the charge-compensating cation (K^+). *It is clear that the nature of the boron source is a factor governing the structural features of SBA-15–SO_3H.* The important crystal parameters of the samples are presented in Table 1. The d-spacing of the samples are compatible with the hexagonal p6mm space group. When compared to siliceous SBA-15–SO_3H, the d-spacing values of SBA-15–SO_3H–$B(OH)_3$, TIB, KBH_4 are slightly low. The lowering of d-spacing of these samples suggests the successful isomorphous substitution of B into the siliceous framework of SBA-15–SO_3H by direct synthesis method. The lowering of d-spacing is due to the shortening of M–O bond distance by B insertion (the atomic size of boron is smaller than Si) in the framework, which brings a decrease in unit cell parameter. Similarly, the unit cell parameter a_0 calculated for (100) plane is found to decrease due to B incorporation.

The high-angle XRD spectra show a broad reflection at $2\theta \sim 22°$ due to amorphous silica (Fig. 2). Because of the low loading of boron sources, the peaks related to the boron source are hardly visible. Indeed, as already suggested by the FT-IR analyses, the boron atoms in the samples are mainly engaged in the formation of borosiloxane bridges, and the crystallization of boron source is strongly hindered [11].

The IR spectra in the 400–4000 cm^{-1} region contain a series of bands that are characteristic of the SiO_4

Table 1 Physicochemical and textural properties of the catalyst samples determined by XRD, ICP/OES, BET/BJH and titration methods

Samples	d_{100} (nm)	a_{100} (nm)	B% (ICP)[a]	S_{BET} ($m^2\ g^{-1}$)	d_{pore} (nm)	V_{pore} (cm^3/g)	Acidity ($mmolH^+/g$)[b]
SBA-15–SO_3H	9.97	11.51	–	623.3	5.57	0.872	0.907
SBA-15–SO_3H–$B(OH)_3$	9.91	11.44	0.021	494.2	5.50	0.679	1.218
SBA-15–SO_3H–TIB	9.91	11.44	0.023	419.1	5.48	0.574	1.183
SBA-15–SO_3H–KBH_4	9.29	10.73	0.079	357.9	5.26	0.471	1.005

[a]SD is ±0.001

[b]SD is ± 0.023

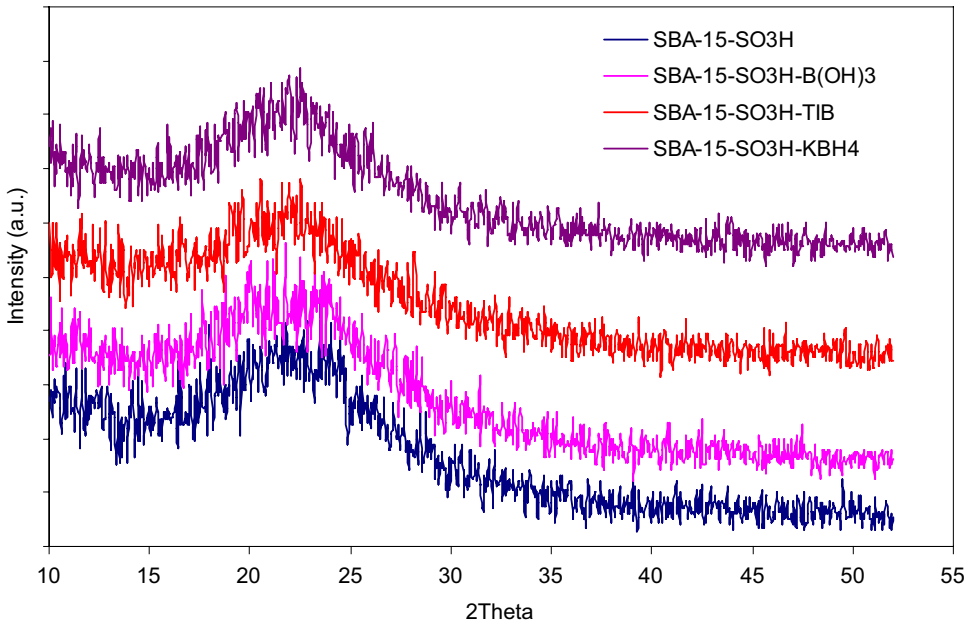

Fig. 2 High-angle XRD spectra for bare SBA-15–SO_3H and boron incorporated SBA-15–SO_3H samples

tetrahedron unit and its modification by introduction of boron and sulfonic acid groups (Figs. 3, 4). All spectra are characterized by the typical bands associated with the Si–O bonds at 1120–1020 cm^{-1} (υ Si–O), 840–790 cm^{-1} (ρ Si–O–Si), and 460–400 cm^{-1} (δ Si–O–Si). Absorption at 920–950 cm^{-1} (υ Si–OH) and at 1620 cm^{-1} (δ H–O–H) suggest the presence of terminal hydroxyl groups as well as absorbed water. Different from the spectra of SBA-15 and B–SBA-15 (Fig. 3), the boarding of the band between 1000 and 1200 cm^{-1} can be observed since the peaks at 1190 and 1036 cm^{-1} assigning to SO_3H groups overlap with those of the silica framework (Fig. 4). The presence of boron gives

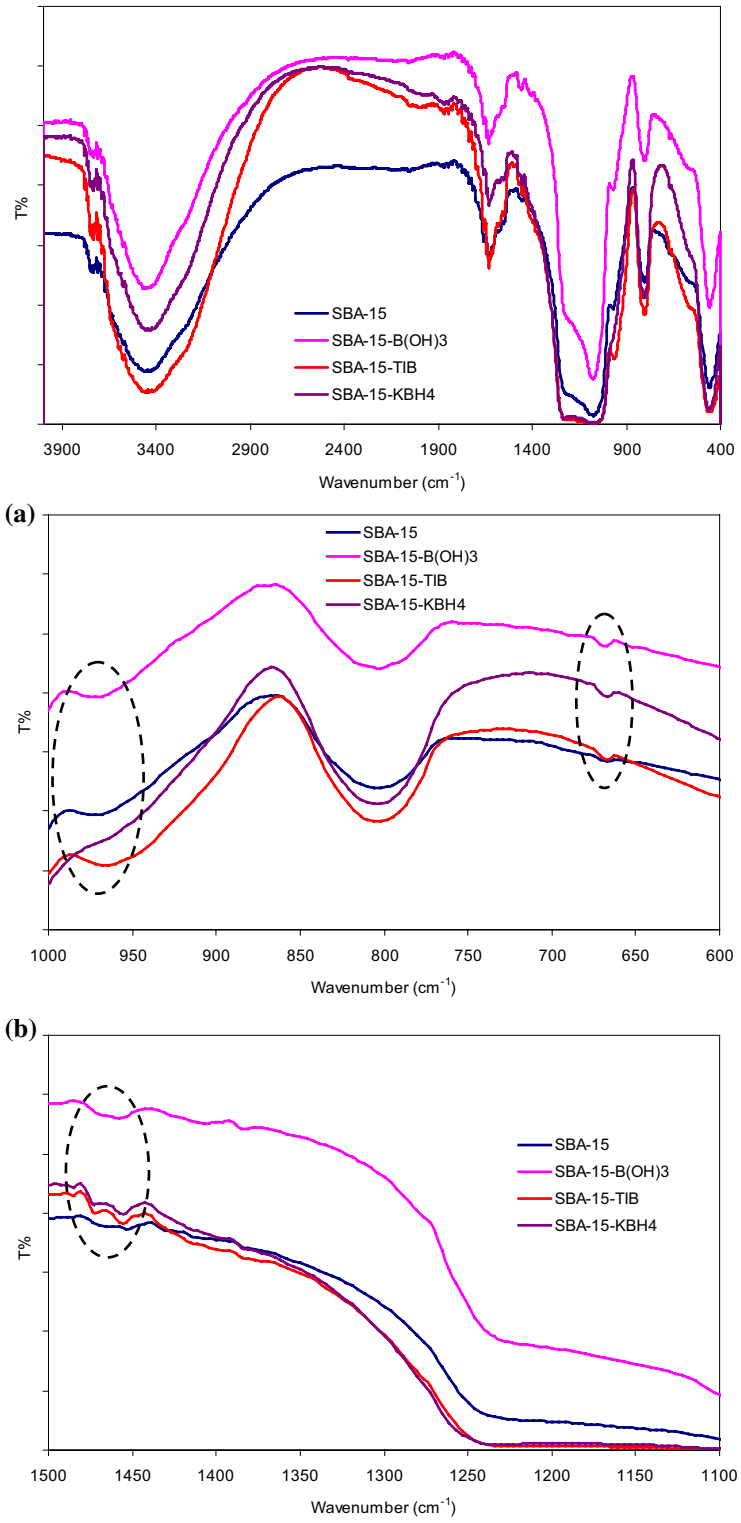

Fig. 3 FT-IR spectra for bare SBA-15 and boron incorporated SBA-15 samples. **a** The *inset* of Fig. 3 between 600 and 1000 cm^{-1}. **b** The *inset* of Fig. 3 between 1100 and 1500 cm^{-1}

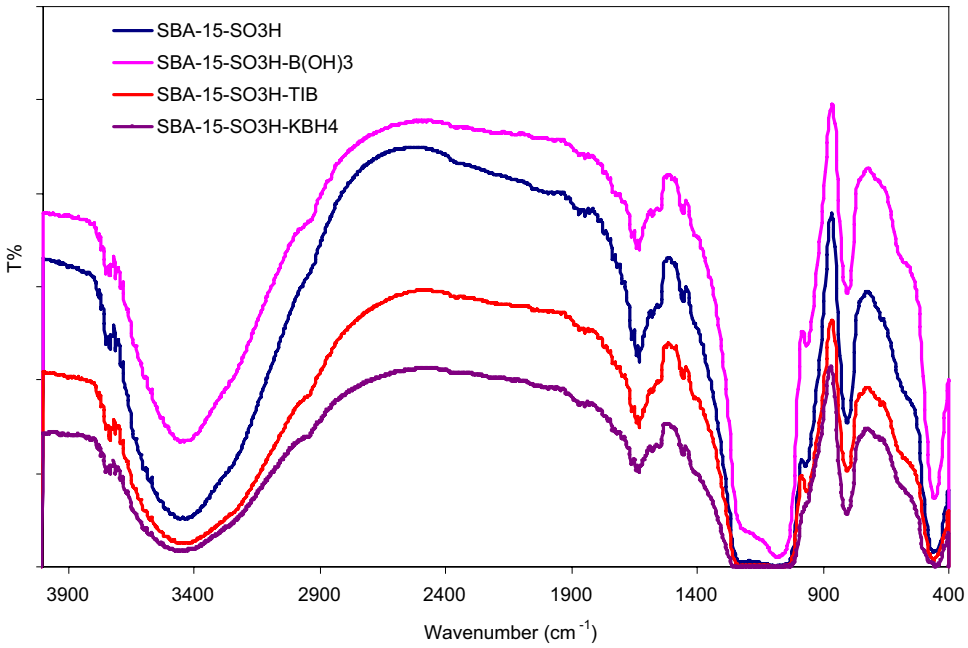

Fig. 4 FT-IR spectra for sulfonic acid functionalized samples (SBA-15–SO_3H and B–SBA-15–SO_3H)

rise to peaks at 1500–1300 cm^{-1} (υ B–O) and at 1195 cm^{-1} (δ B–OH) [11]. According to the literature, the bands at 930–915 cm^{-1} (υ B–O–Si) and at 675 cm^{-1} (δ B–O–Si) are due to borosiloxane bridges. Furthermore the band at 920 cm^{-1} is attributed to tetracoordinated boron, while the band at 1380 cm^{-1} to tricoordinated boron [2]. Since the peaks belonging to borosiloxane bridges are hardly distinguished, we examined the FT-IR spectra of the samples piecemeal (Fig. 3a, b) to ascertain the structural change of boron incorporated samples. In the first part, the band at 675 cm^{-1} is essentially absent for the pure-silica analogue; however, the shoulder band at ~980 cm^{-1} is weakly visible (Fig. 3a). This band at ~980 cm^{-1} is also due to the silanol group present in the calcined pure SBA-15-SO_3H. In the second part of the FT-IR spectra, other bands (υ B-O) are also appeared between 1450 and 1500 cm^{-1} assigning the presence of boron differently from pure silica analogue.

Because of three-coordinate boron's electron-deficient nature, it is easily attacked by nucleophilic molecules like water. Therefore, boron parts of the material quickly hydrolyze rather than condense to form borosiloxane. During heat treatment, some of the boron source condensed with the siloxy-network to form borosiloxane, and some was lost by evaporation at high calcination temperature (500 °C) [12]. This change for calcined and uncalcined SBA-15–$B(OH)_3$ is proven in Fig. 5. It was concluded from Fig. 5 that, all of the bands around at 980 and 675 cm^{-1} and between 1300 and 1500 cm^{-1} disappeared after calcination. According to the work of Soraru et al. [11] that during the sol–gel process to obtain SiO_2–B_2O_3 glasses from $Si(OR)_4$, R≡Me, Et, borosiloxane bridges are initially formed in solution through the reaction:

$$\equiv Si - OH + HO - B = \rightarrow \equiv Si - O - B = + H_2O \quad (1)$$

Then, the condensation reactions lead to an increase of the water concentration that can hydrolyze back the borosiloxane bonds so no B-O-Si bonds are found in the final gel. According to this model, the observed presence of a shoulders around at 675 and 1450 cm^{-1} in the boron incorporated samples could be ascribed to i; the borosiloxane bridges formed in solution that are not completely hydrolyzed during the final stages of the sol–gel process or ii; a higher stability of the B–O–Si bridges toward hydrolysis. In the case of TIB (Fig. 3b), the bands between the 1450 and 1500 cm^{-1} are more distinct compared to $B(OH)_3$. Because the presence of organic groups instead of –OH groups close to borosiloxane bridges could act as an insitu protection of the borosiloxane bonds from the water attack. Due to their higher steric hindrance, protection given from the isopropyl moieties should be higher compared to that provided by hydroxyl groups [11].

ICP–OES (inductively coupled plasma-optical emission spectrometry) was used for boron estimation and the final boron content present in the obtained samples, SBA-15–SO_3H–$B(OH)_3$, SBA-15–SO_3H–TIB, and SBA-15–SO_3H–KBH_4 are shown in Table 1. *According to the results obtained from ICP-OES analyses, KBH_4 was the boron source that led towards the highest degree of boron incorporation into the SBA-15 framework.*

The structure and morphology of the SBA-15–SO_3H and SBA-15–SO_3H–$B(OH)_3$, SBA-15–SO_3H–TIB, and SBA-15–SO_3H–KBH_4 samples were analyzed by scanning electron microscopy. The typical SEM images of SBA-15–SO_3H and B–SBA-15–SO_3H samples are presented

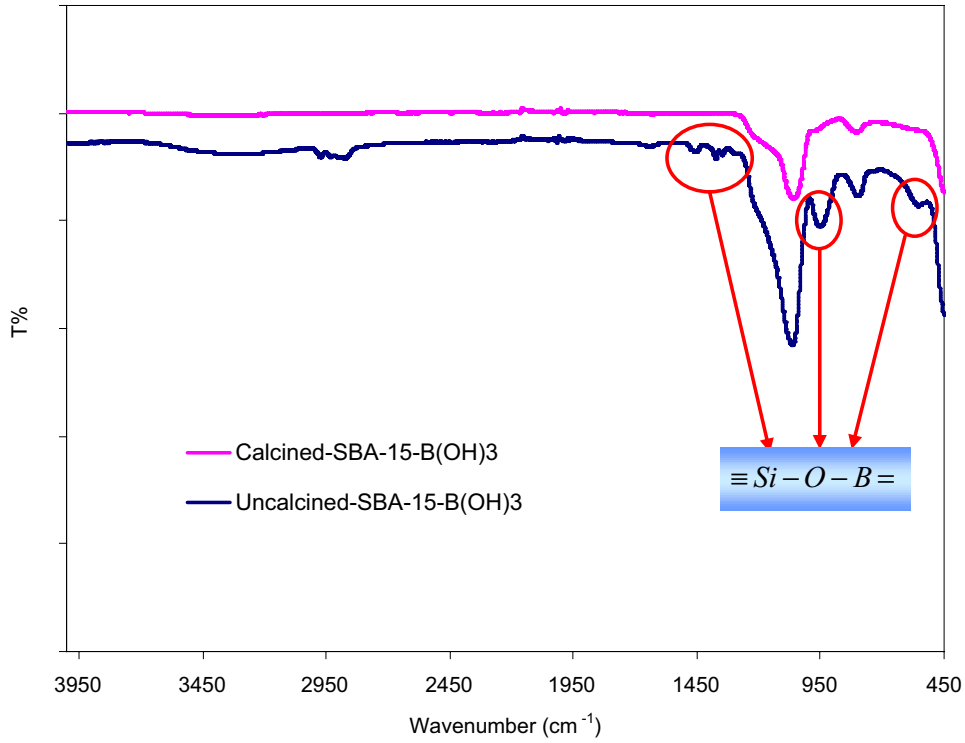

Fig. 5 FT-IR spectra for calcined and uncalcined B–SBA-15 samples

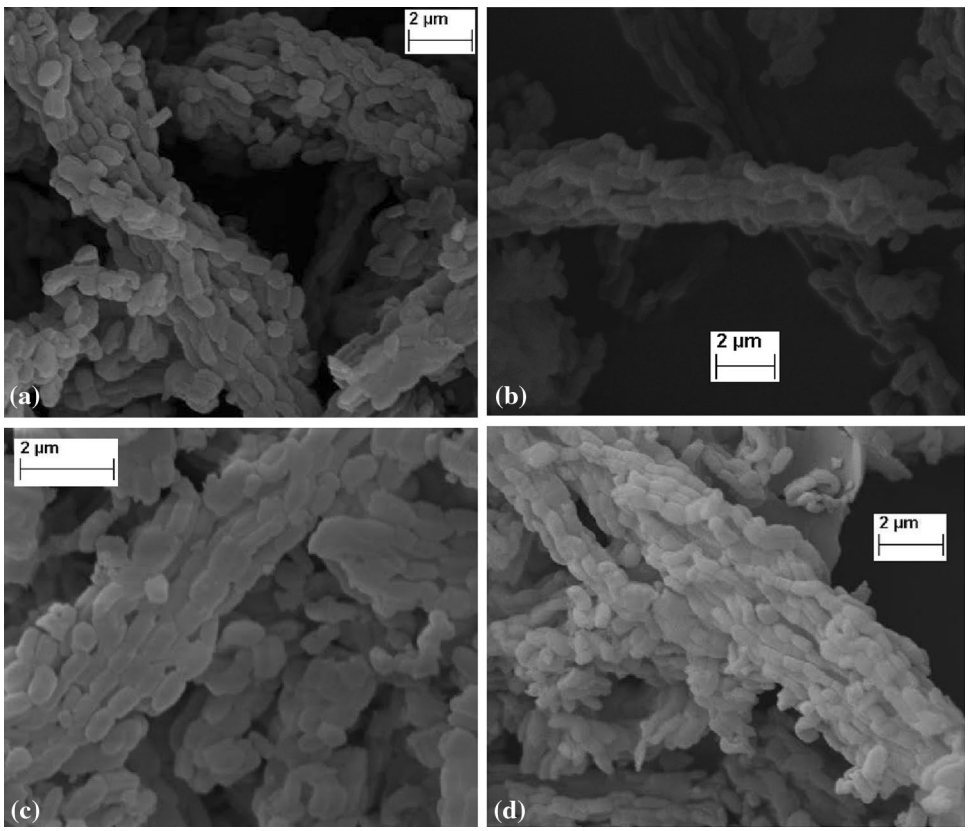

Fig. 6 SEM images of the bare SBA-15-SO_3H (**a**). Boron incorporated SBA-15-SO_3H with $B(OH)_3$ (**b**). TIB (**c**). KBH_4 (**d**) as boron sources

in Fig. 6a–d, respectively. In the case of SBA-15–SO_3H (Fig. 6a), it shows many rope-like domains that aggregate into a microstructure with relatively uniform size, which are agree with the previous reports. Each rope-like structure consists of packages of number of segmental fibers. In the case of B–SBA-15–SO_3H, there is no significant change

in morphology since the boron content is low. Even though the average size of rope-like domains does not change much, for B–SBA-15–SO_3H samples there is little change in morphology like turning to elongated hexagonal prism.

Figure 7 illustrates the N_2 adsorption/desorption isotherms of SBA-15–SO_3H–$B(OH)_3$, SBA-15–SO_3H–TIB, and SBA-15–SO_3H–KBH_4, and pure SBA-15–SO_3H, the latter included for comparison. These four isotherms reveal the shape of type IV, typical of mesoporous materials. However, some differences can be envisaged. All of the isotherms are very similar with a steep jump at $p/p_o = 0.6–0.7$ from capillary condensation into the mesopores [8]. The corresponding jump for SBA-15–SO_3H–KBH_4 differs slightly related to lower pore volumes. This might result from the more interaction of boron with the silica structure as experienced with the other experimental results. The inset of Fig. 7 illustrates the pore-size distribution curves calculated from the desorption branch of the BJH model. Apparently, all the samples prepared with different boron sources have similar mean pore sizes of 5.2–5.6 nm. All the samples possess relatively high BET surface areas (Table 1) and mesopores. However, pore-size distributions become slightly broader with the boron incorporation.

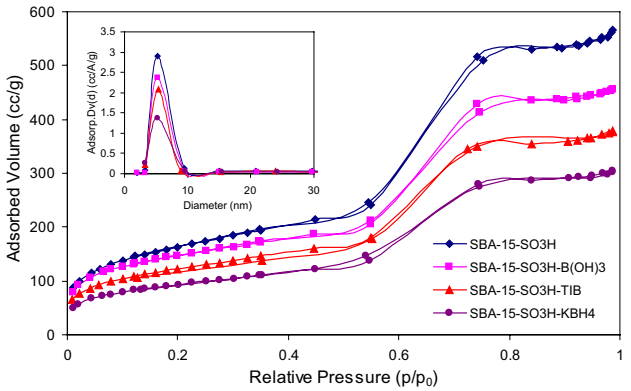

Fig. 7 Nitrogen adsorption–desorption isotherms of bare and boron incorporated SBA-15–SO_3H samples. The *inset* shows the corresponding BJH pore size distributions

It is well known that propionic acid–methanol esterification reaction is a consecutive reaction. As can be seen from Fig. 8, all the B–SBA-15–SO_3H catalysts show significant activity compared to SBA-15–SO_3H, indicating that the acid sites created by boron incorporation are responsible for the catalytic activity. This result can be proved with the acid capacity values shown in Table 1. However, among the B–SBA-15–SO_3H catalysts, SBA-15–SO_3H–$B(OH)_3$ shows the maximum activity compared to other catalysts studied but has the minimum boron content among the boron incorporated samples. Furthermore, the difference in acid capacity values of the catalysts is not as high as reaction conversions. *In our opinion, the boron sources, which are being added during synthesis, act as a second structure agent material except non-ionic surface active material (Pluronic P123). After calcination, the template molecules are removed from the substrates to leave pores and the cavities in the monolayer coating. The size and the shape of the cavities could be varied by the second template, i.e., boron source*. Herein, we describe a design strategy for imprint-coated, functionalized ordered mesoporous acid catalyst through surface molecular imprinting [13, 14].

$$CH_3CH_2COOH + CH_3OH \rightleftarrows CH_3COOCH_2CH_3 + H_2O \quad (2)$$

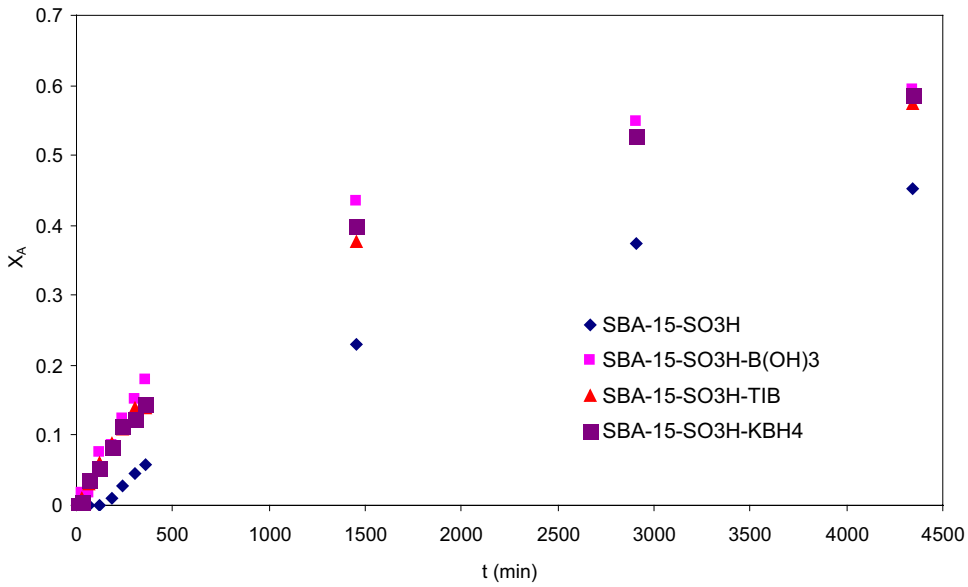

Fig. 8 Reaction conversions for the esterification of propionic acid with methanol (60 °C; PA:MeOH molar ratio: (1:1); catalyst: 0.5 g, stirring rate: 500 rpm, solvent: 1,4-dioxane, total volume: 100 mL)

The rate of model reaction (2) by using the homogeneous model can be written as

$$-\frac{dC_{PA}}{dt} = k_1 C_{PA} C_{MeOH} - k_2 C_{MeP} C_W \quad (3)$$

For a molar ratio of $M = C_{PA,0}/C_{MeOH,0} = 1$ and initial concentrations methylpropionate and water, $C_{MeP} = C_W = 0$; Eq. (3) can be written to give the following equation in terms of the fractional conversion of the propionic acid.

$$\frac{dX_{PA}}{dt} = k_1 \left(1 - X_{PA}\right)^2 - k_2 \left(X_{PA}\right)^2 \quad (4)$$

For a molar ratio of $M = C_{PA,0}/C_{MeOH,0} = 1$ Eq. (4) can be integrated to give the following equation,

$$\ln \frac{X_{PA,e} - \left(2X_{PA,e} - 1\right)X_{PA}}{X_{PA,e} - X_{PA}} = 2k_1 \left(\frac{1}{X_{PA,e}} - 1\right) C_{PA,0} t \quad (5)$$

where X_{PA}, fractional conversion of propionic acid,

$$X_{PA} = \frac{C_{PA,0} - C_{PA}}{C_{PA,0}} \quad (6)$$

Thus, plot was made of the left-hand side versus time for Eq. (5) to determine the slope of the line from which the values of k_1 was calculated. Kinetic plots for the reaction between methyl alcohol and propionic acid; are shown in Fig. 9. The values of k_1 for the catalysts SBA-15–SO_3H, SBA-15–SO_3H–$B(OH)_3$, SBA-15–SO_3H–TIB, and SBA-15–SO_3H–KBH_4 were found to be 2.31×10^{-4}, 5.88×10^{-4}, 5.74×10^{-4} and 5.83×10^{-4} $dm^3\ mol^{-1}\ min^{-1}$, respectively. Figure 9 shows the suitability of this model (Eq. 5) for representation of the rate data. The data fall on straight lines for SBA-15–SO_3H and B–SBA-15–SO_3H catalyst having different boron sources confirming the applicability of the model for this reaction.

Reusability is likely to be a key factor in the improvement of process economics. For this reason, the reusability property of the catalysts is worthy of study. To determine the reusabilities of SBA-15–SO_3H–$B(OH)_3$ and SBA-15–SO_3H–TIB, the consecutive esterification reactions were repeated three times with the same catalysts. Catalytic activity and conversion for each cycle are given in Fig. 10. Catalyst activity decreased about 10% after the each cycles because of the lack of catalyst mass. Thus the mesoporous B–SBA-15–SO_3H catalysts described herein have great potential to be stable and highly active recyclable solid acid catalysts.

4 Conclusion

We successfully combined the hydrothermal synthesis and post-functionalization to obtain a new versatile mesoporous solid acid catalyst, B–SBA-15–SO_3H, by using three different boron sources. We characterized the mesoporous and amorphous character of the materials as well as the incorporation of the boron into the SBA-15 even at low SiO_2/B_2O_3 ratio: 30. Catalytic tests showed the efficiency of these materials for the catalysis of sustainable reaction (esterification of propionic acid with methanol). Boron incorporated SBA-15–SO_3H catalysts demonstrated high reactivity as well as reasonable recyclability for the esterification reaction, and are there with promising heterogeneous acid catalyst.

We have also find that such boron incorporated, functionalized, ordered mesoporous acid catalysts exhibit different binding selectivity for the target reaction according to boron source. In totally, the success of our approach is

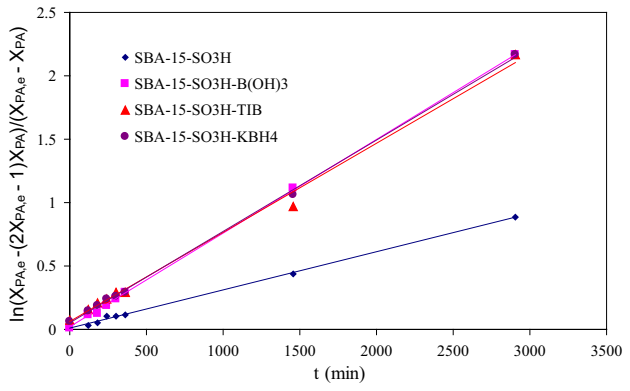

Fig. 9 Suitability of homogeneous model assuming second order reaction kinetics for the reaction between methanol with propionic acid

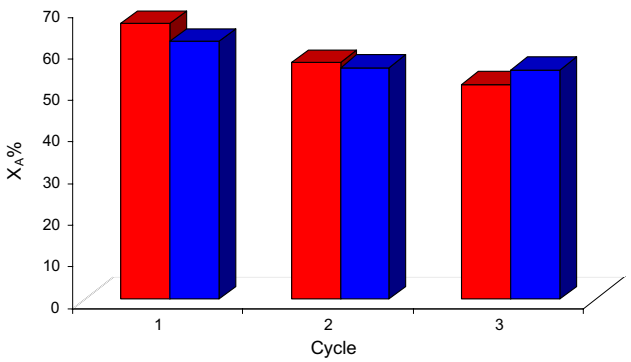

Fig. 10 Kinetic plots of recycling test of SBA-15–SO_3H–$B(OH)_3$ (represented by *red column*) and SBA-15–SO_3H–TIB (represented by *blue column*) in the esterification reaction of methanol with propionic acid. (Color figure online)

built upon the unique environments of ordered, hexagonally packed mesopore surfaces for conducting surface imprinting.

Acknowledgements This work was supported by The Commission of Scientific Research Projects of Uludag University, Project Number: OUAP(F)-2015/21. The authors thank Prof. Dr. Ramis Mustafa Öksüzoğlu for assistance in XRD characterization.

References

1. D. Rath, S. Rana, K.M. Parida, RSC Adv. **4**, 57111–57124 (2014)
2. D. Trong On, P.N. Joshi, S. Kallaguine. J. Phys. Chem **100**, 6743–6748 (1996)
3. I. Eswaramoorthi, A. K. Dalai. Micro. Meso. Mater. **93**, 1–11 (2016)
4. U. Oberhagemann, I. Kinski, I. Dierdorf, B. MArler, H. Gies, J. Non-Cryst. Solids **197**, 145–153 (1996)
5. Y. Zheng, J. Li, N. Zhao, W. Wei, Y. Sun, Micro. Meso. Mater. **92**, 195–200 (2006)
6. D. Srinivas, L. Saikia, Catal. Surv. Asia. **12**, 114–130 (2008)
7. D. Brühwiler, Nanoscale **2**, 887–892 (2010)
8. R. van Grieken, J.M. Escola, J. Moreno, R. Rodriguez. Chem. Eng. J. **155**, 442–450 (2009)
9. S. Wu, Y. Han, Y.C. Zou, J.W. Song, L. Zhao, Y. Di, S.Z. Liu, F. S. Xiao. Chem. Mater. **16**, 486–492 (2004)
10. Y. Sarıkaya, *Physical Chemistry*, 10th edn. (Gazi Publishing, Ankara, Turkey, 2011), p. 664 **(In Turkish)**
11. G.D. Soraru, N. DAllabona, C. Gervais, F. Babonneau, Chem. Mater. **11**, 910–919 (1999)
12. T. Xiu, Q. Liu, J. Wang, J. Mater. Res. **22**, 1834–1838 (2007)
13. Y. Shin, J. Liu, L.Q. Wang, Z. Nie, W.D. Samuels, G.E. Fryxell, G.J. Exarhos, Angew. Chem. Int. Ed. **39**, 2702–2707 (2000)
14. S. Dai, M.C. Burleigh, Y. Shin, C.C. Morrow, C.E. Barnes, Z. Xue, Angew. Chem. Int. Ed. **38**, 1235–1239 (1999)